High Microfilament Concentration Results in Barbed-end ADP Caps

Paul A. Dufort and Charles J. Lumsden*
Membrane Biology Group and Department of Medicine, University of Toronto, Toronto, Canada M5S 1A8

ABSTRACT Current theory and experiments describing actin polymerization suggest that site-specific cleavage of bound nucleotide following F-actin filament formation causes the barbed ends of microfilaments to be capped first with ATP subunits, then with ADP bound to inorganic phosphate (ADP·P_i) at steady-state. The barbed ends of depolymerizing filaments consist of ADP subunits. The decrease in stability of the barbed-end cap accompanying the transition from ADP·P_i to ADP allows nucleotide hydrolysis and subsequent loss of P_i to regulate F-actin filament dynamics. We describe a novel computational model of nucleotide capping that simulates both the spatial and temporal properties of actin polymerization. This model has been used to test the effects of high filament concentration on the behavior of the ATP hydrolysis cycle observed during polymerization. The model predicts that under conditions of high microfilament concentration an ADP cap can appear during steady-state at the barbed ends of filaments. We show that the presence of the cap can be accounted for by a kinetic model and predict the relationship between the nucleotide concentration ratio [ATP]/[ADP], the F-actin filament concentration, and the steady-state distribution of barbed-end ADP cap lengths. The possible consequences of this previously unreported phenomenon as a regulator of cytoskeletal behavior are discussed.

INTRODUCTION

Actin is a ubiquitous, highly conserved polymeric protein found in large concentrations in the periphery of eukaryotic cells. Actin filaments provide structural support and are key components in determining the motile and viscoelastic properties of the cell. A large network of regulatory proteins acts in concert with intracellular messengers to dynamically remodel the actin cytoskeleton, producing a highly organized cooperative system that is the primary effector of cell deformation processes (Korn, 1982; Stossel et al., 1985; Pollard and Cooper, 1986).

The monomeric form of actin (G-actin) possesses a nucleotide binding site and one high-affinity divalent cation binding site. Under physiological salt concentrations (100 mM KCl and 1 mM Mg^{2+}), G-actin spontaneously polymerizes into long helical filaments (F-actin). These filaments are polarized, such that polymerization proceeds more rapidly at one end (the "barbed" end) than at the other (the "pointed" end) (Carlier, 1991).

In order to understand the complex network of proteins and ligands that regulate the actin cytoskeleton, it is essential first to understand how the kinetics of the polymerization process itself are regulated. The most widely received model at present was originally outlined by Korn et al. (1987) and is briefly summarized in the following four paragraphs.

The nucleotide binding site of G-actin may be occupied by either ATP or ADP. Polymerization of ADP·G-actin is consistent with the reversible nucleation-elongation process for helical filaments described by Oosawa and Asakura (1976). According to Oosawa and Asakura, polymerization occurs more rapidly at the barbed end of the filament than at the pointed end; however, the reaction is reversible so dissociation is more rapid at the barbed end as well, and the resulting critical concentration at both ends is equal.

Polymerization of ATP·G-actin is more complex (Korn et al., 1987). Following the association of ATP monomers with the barbed ends of filaments, the bound ATP is rapidly cleaved to ADP·P_i. The rate of cleavage of ATP on a given subunit is strongly dependent on the type of nucleotide bound to immediately adjacent subunits. Cleavage is approximately 10^4 times more probable if the ATP subunit lies adjacent to an ADP or ADP·P_i subunit than if it is surrounded by other ATP subunits. The more probable type of cleavage is called vectorial hydrolysis, because it results in an interface between newly polymerized ATP and older ADP·P_i subunits. This interface moves rapidly toward filament ends. The less probable cleavage type is called random hydrolysis, because it can occur anywhere within a region of ATP subunits. After hydrolysis, the P_i bound to ADP·P_i subunits is released over a time period roughly 10^3 times longer than that required for hydrolysis, leaving F-actin subunits bound only to ADP. The release of P_i from ADP·P_i subunits occurs randomly at any position.

When ATP·G-actin concentration is high and the rate of association at the barbed ends of filaments far exceeds the rate of cleavage of the bound ATP, a long cap of ATP subunits forms at the barbed ends of filaments. As the monomer pool is depleted and polymerization slows, ATP cleavage consumes the ATP cap leaving a cap of ADP·P_i subunits in its place. Finally, at steady state, random release of P_i causes most of the inner core of subunits to be bound to ADP, while a small cap of ADP·P_i subunits persists at the barbed ends of filaments. A similar sequence of events is thought to occur at the pointed ends of filaments, but the slower polymerization rates at this end have made confirmation of this hypothesis difficult (Korn et al., 1987).

Received for publication 24 May 1993 and in final form 26 August 1993.
Address reprint requests to Charles J. Lumsden at Room 7313, Medical Sciences Building, University of Toronto, Toronto, Ontario, Canada M5S 1A8. Tel.: 416-978-7178; Fax: 416-978-8765.

0006-3495/93/11/1757/10 $2.00

According to the above model, the polymerization of ATP·G-actin consumes a large amount of energy through the hydrolysis of ATP. Korn et al. (1987) have pointed out that this is not usual for noncovalent assembly processes, and have suggested that the most likely reason for this phenomenon is therefore to provide a regulatory switch for actin polymerization. They have further proposed that this regulatory switch could facilitate the formation and destruction of filaments whenever required through a mechanism similar to the dynamic instability observed for microtubules. The crucial determinant in dynamic instability is the type of nucleotide bound to the terminal subunits of filaments. It is therefore essential to establish which type of nucleotides will be present on the tips of actin filaments under different conditions.

Many cytoskeletal remodeling processes associated with phospholipase C-mediated turnover in the phosphatidylinositol pathway consist of two sequential steps. First, rapid hydrolysis of phosphatidylinositol bisphosphate (PIP_2) into diacylglycerol and inositol triphosphate causes intracellular Ca^{2+} stores to be emptied into the cytosol. Raised levels of Ca^{2+} then activate F-actin severing and nucleating proteins, resulting in a several-fold increase in the number of filaments. Second, phosphorylation of phosphatidylinositol and phosphatidylinositol phosphate (PIP) raises PIP_2 levels again, stimulating monomer sequestering proteins to release large amounts of G-actin into the cytosol. The net result of these processes is an extensive polymerization of newly released monomers on to newly formed filament ends (Stossel, 1989).

In order to explore the importance of actin's ATP hydrolysis cycle during this kind of remodeling process, we have conducted a simulation of Korn et al.'s (1987) actin polymerization model under conditions of high filament concentration. We begin this paper with a summary of the computer model and the simulation of actin polymerization. We then review the simulation results, focusing on the formation of small ADP caps at the barbed ends of filaments over an extended period of time and discussing the causes of this phenomenon. We find that our results both support and extend Korn et al.'s (1987) hypothesis. We conclude with a discussion of the potential implications of this phenomenon for regulation of cytoskeletal structure and function in vivo.

MATERIALS AND METHODS

The mechanisms proposed to account for the formation of ATP caps on polymerizing microfilaments were tested with a cellular automaton (CA) method of modeling the actin cytoskeleton (Dufort and Lumsden, 1993). By incorporating both reaction and diffusion in a single framework, the CA method simultaneously solves the kinetic rate equations describing the concentrations of all chemical species and the reaction-diffusion equations describing the emergence of spatial and temporal order. The reaction mechanisms and rate constants used in the simulation described in this paper are listed in Table 1, along with the references from which the rate constants were taken.

Biochemistry in the model

Proteins, ligands, and reactions were chosen to incorporate the mechanisms used in the model of actin polymerization proposed by Korn et al. (1987). The proteins and ligands consisted of G-actin monomers and F-actin filaments, the divalent cation Mg^{2+}, the nucleotides ATP and ADP, and the ATP hydrolysis product P_i. The effects of Ca^{2+} have not been included because actin is thought to be bound primarily to Mg^{2+} under physiological conditions (Korn, 1982).

The model's database organized the molecular species into two classes. Class 1 contained the macromolecules G-actin and F-actin, whose motion was simulated explicitly, while Class 2 contained the smaller molecules ATP, ADP, Mg^{2+}, and P_i. The model assigned Class 2 reactants an infinite diffusive mobility and distributed them homogeneously throughout the simulation volume at all times. This approximation is justified by the large diffusion constant for these small molecules and the small size of the simulation volume (600 nm on each side) (Dufort and Lumsden, 1993).

The reaction mechanisms and kinetic data for these species can be summarized as follows.

Class 1 reactants

Actin polymerization

G-actin monomers could bind to filament ends and F-actin subunits could dissociate from filament ends. The rate constants varied with the cation and nucleotide bound to the associating or dissociating subunit (Pollard, 1986), and with the end of the filament (barbed or pointed) involved (Carlier, 1991). G-actins without a bound cation and a bound nucleotide could not bind to filaments (Korn, 1982). F-actin subunits with bound ADP·P_i dissociated with the same rate constant as ATP subunits (Korn et al., 1987). Reported rate constants vary widely depending on the ionic salt concentrations used to induce polymerization, especially Mg^{2+}, Ca^{2+}, and KCl. All of our modeling runs used rate constants from experiments conducted in or very close to 100 mM KCl, 1 mM Mg^{2+}, and 0.1 μM Ca^{2+}. These values were chosen for their similarity with intracellular ionic conditions (Nowak and Goody, 1988).

Class 2 reactants

Cations

Each actin subunit in the model could bind either one Mg^{2+} or no cation (Korn, 1982). Binding and dissociation of cations was only permitted for G-actin (Estes et al., 1987). F-actin subunits were assumed to be bound to Mg^{2+}. Monomers without a bound cation could not nucleate or polymerize (Pollard and Cooper, 1986). Rate constants for cation binding depended on the type of nucleotide bound to the monomer (Carlier, 1991). This scheme was based on the first-order model of Estes et al. (1987) for the high affinity cation binding site of actin.

Nucleotides

Each actin subunit in the model could bind either one ATP or one ADP, or no nucleotide (Korn, 1982). Binding and dissociation of nucleotides was only permitted for G-actin (Korn, 1982). Monomers without a bound nucleotide could not nucleate or polymerize (Korn, 1982). Rate constants for nucleotide binding depended on the type of nucleotide and the type of cation bound to the monomer (Kinosian et al., 1993). Hydrolysis of bound ATP to ADP·P_i could only occur on F-actin subunits (Korn et al., 1987; Carlier et al., 1987). The nucleotide concentrations in all of the modeling runs described in this paper were fixed at 200 μM ATP and 20 μM ADP in order to approximate physiological conditions.

ATP hydrolysis

ATP bound to F-actin subunits in the model could be hydrolyzed to form ADP·P_i (Carlier and Pantaloni, 1986). The probabilities governing this pro-

TABLE 1 Reactions, mechanisms, and rate constants used in the simulation

Number	Reaction	Rate constants k_+	Rate constants k_-	Reference
		$\mu M^{-1}\ s^{-1}$	s^{-1}	
1	$G{\cdot}ATP + Mg \underset{k_-}{\overset{k_+}{\rightleftharpoons}} G{\cdot}ATP{\cdot}Mg$	0.36	0.01	1
2	$G{\cdot}ADP + Mg \underset{k_-}{\overset{k_+}{\rightleftharpoons}} G{\cdot}ADP{\cdot}Mg$	21.0	0.04	2
3	$G{\cdot}Mg + ATP \underset{k_-}{\overset{k_+}{\rightleftharpoons}} G{\cdot}ATP{\cdot}Mg$	1.1	0.005	3, 4*
4	$G{\cdot}Mg + ADP \underset{k_-}{\overset{k_+}{\rightleftharpoons}} G{\cdot}ADP{\cdot}Mg$	1.2	0.033	3, 4*
5	$F{\cdot}ATP{\cdot}Mg \xrightarrow[(random)]{k_+} F{\cdot}ADP{\cdot}P_i{\cdot}Mg$	$0.001\ s^{-1}$		5
6	$F{\cdot}ATP{\cdot}Mg \xrightarrow[(vector)]{k_+} F{\cdot}ADP{\cdot}P_i{\cdot}Mg$	$12.3\ s^{-1}$	(Barbed)	5
7	$F{\cdot}ATP{\cdot}Mg \xrightarrow[(vector)]{k_+} F{\cdot}ADP{\cdot}P_i{\cdot}Mg$	$1.3\ s^{-1}$	(Pointed)	5
8	$F{\cdot}ADP{\cdot}P_i{\cdot}Mg \xrightarrow{k_-} F{\cdot}ADP{\cdot}Mg + P_i$		0.0055	6
9	$G{\cdot}ATP{\cdot}Mg + F_n^B \underset{k_-}{\overset{k_+}{\rightleftharpoons}} F_{n+1}^B$	5.2	0.36	2
10	$G{\cdot}ATP{\cdot}Mg + F_n^P \underset{k_-}{\overset{k_+}{\rightleftharpoons}} F_{n+1}^P$	1.3	0.8	7
11	$G{\cdot}ADP{\cdot}Mg + F_n^B \underset{k_-}{\overset{k_+}{\rightleftharpoons}} F_{n+1}^B$	0.9	1.8	8
12	$G{\cdot}ADP{\cdot}Mg + F_n^P \underset{k_-}{\overset{k_+}{\rightleftharpoons}} F_{n+1}^P$	0.14	0.28	7‡

Abbreviations used: Mg = magnesium, ATP = adenosine triphosphate, ADP = adenosine diphosphate, G = G-actin, F = F-actin (B = barbed end, P = pointed end, n = filament contains n subunits).
References: 1: Estes et al. (1987), 2: Carlier (1991), 3: Nowak and Goody (1988), 4: Kinosian et al. (1993), 5: Carlier et al. (1987), 6: Carlier and Pantaloni (1986), 7: Pollard (1986), 8: Pollard and Cooper (1986).
*The nucleotide dissociation rate constants, taken from Kinosian et al. (1993), have been increased 10-fold to account for the presence of 100 mM KCl.
‡These rate constants have been adjusted slightly (10%) to ensure that the critical concentration of ADP-actin is the same at both ends of the filament. The adjustment is well within the published error in the constants (Pollard, 1986).

cess depended on the type of nucleotide bound to the adjacent subunits on the filament. The model incorporated a constant rate of hydrolysis that could occur at any random location on the filament, but hydrolysis on ATP subunits adjacent to ADP·P_i subunits occurred far more rapidly (this process is called vectorial hydrolysis) (Korn et al., 1987). Vectorial hydrolysis toward the barbed end occurred more rapidly than toward the pointed end (Carlier et al., 1987).

P_i release

P_i could be released from ADP·P_i·F-actin subunits at random to form ADP subunits (Carlier and Pantaloni, 1986).

The cellular automaton model

The basic simulation method and its physical justification have recently been described (Dufort and Lumsden, 1993). We give here a summary of the method and its implementation for nucleotide cap modeling. The chemical reactions occurred in a three-dimensional cellular automaton whose sites formed a cubic lattice. Several discrete variables were associated with each lattice site representing the presence or absence of a molecule, the species and orientation of the molecule, the presence or absence of bound nucleotides and cations, and a list of other proteins to which the molecule was bound. At each time step, every class 1 molecule in the lattice was given the opportunity to react with neighboring molecules and to diffuse to an adjacent site.

Diffusion was implemented by having every molecule choose an adjacent site at random. A random number was then generated and compared to the probability of an object of this molecule's size diffusing to the adjacent site in one time step. If the random number was less than the probability, the molecule moved to the new site. If the number was greater than the probability, the molecule had to wait until the next time step, when the lottery process was repeated.

Molecules could move to any of 26 adjacent sites. To respect the strong steric repulsion between molecules in close proximity, no lattice site could be occupied by more than one molecule at a time. The lattice spacing parameter Δx (the shortest distance separating each lattice site) was set to 7 nm to reflect the approximate distance between two F-actin filaments (Holmes et al., 1990).

Calculation of molecular diffusion probabilities required the choice of a suitable value for the cytoplasmic viscosity. A value of $\eta = 55$ centiPoise was chosen based upon the work of Jacobson and Wojcieszyn (1984). The diffusion constant for each Class 1 reactant was then calculated as $D = kT/f$, where T is temperature and f is the molecular friction coefficient. Formulae for the friction coefficients in terms of molecular size, shape, and cytoplasmic temperature and viscosity were taken from Tanford (1961). The probability for motion was calculated by comparing the expected root-mean-square displacement of a molecule having diffusion coefficient D after one time step Δt with the distance between the old site and the new site Δx. A value $\Delta t = 10^{-5}$ s was chosen to maximize simulation speed while simultaneously ensuring that the simulation would accurately solve the diffusion equation (Dufort and Lumsden, 1993). Rotational diffusion was handled in a manner analogous to translational diffusion.

Chemical reactions for Class 1 molecules were implemented by having each reactant A scan the lattice site pointed to by its orientation vector. If this site was occupied by molecule B, then the probability of a reaction between A and B was retrieved from a table and compared to a random number to determine if the reaction would take place. If A and B did react

to form a new species $A \cdot B$, then for as long as the two molecules remained bound they were constrained to rotate and translate through the lattice together as a single unit. At each subsequent time step the reverse reaction probability was compared to a random number to determine if the two molecules would dissociate. The reaction probabilities were calculated in terms of experimentally determined rate constants and the cellular automaton lattice spacing Δx and time step Δt (Dufort and Lumsden, 1993).

Class 2 molecules were represented by an average concentration field that was constant throughout the lattice. At each time step every Class 1 reactant A was given the opportunity to react with each concentration field C by comparing the forward reaction probability to a random number. If the reaction took place, then the state of the real molecule A was modified to reflect this new status, and subsequent reactions involving A whose outcomes depended on the presence of C took this status into account. On each subsequent step, A was given an opportunity to lose C via comparison of the reverse reaction probability with a random number.

Simulation

The simulation of actin polymerization and subsequent hydrolysis of ATP was performed on a cubic automaton lattice measuring 600 nm (85 lattice sites) on each side. This size permitted simulation of a sufficient number of molecules to ensure statistically significant tests of the Korn et al. model, while simultaneously maintaining a tolerable program execution time (10 days per simulation run). The lattice was seeded with 800 nM (104 filaments) of F-actin, each filament seed measuring 15 subunits in length and 25 μM of G-actin (2459 monomers). These values were chosen for their consistency with intracellular conditions during cell activation, after extensive filament severing has occurred, and large quantities of G-actin have been released by monomer sequestering proteins (Stossel, 1989). The size of the simulation lattice and the concentrations of actin used also ensured that polymerizing filaments were not prevented from further growth, because they had reached the borders of the lattice. Filament seeds were placed at steady state prior to the addition of the monomers and so consisted of 13 ADP subunits with a small ADP·P_i cap (two subunits) at the barbed end. This assumption is also consistent with conditions expected during cell activation after extensive filament severing.

The CA was simulated on a Silicon Graphics (Mountainview, CA) Crimson VGX workstation for 60 s of model time (6×10^6 iterations). Throughout the simulation, the entire contents of the lattice were saved at intervals of 0.01 s (10^3 iterations) for the first 5 s, and every 0.1 s thereafter (10^4 iterations), so that the change in the nucleotide distribution over time could be visualized and the concentrations of all molecular species could be followed in detail. These time intervals were chosen because few reactions took place over time intervals smaller than this.

RESULTS AND DISCUSSION

The time course of polymerization for the three species of F-actin subunits (ATP, ADP·P_i, and ADP) showed strong differences (Fig. 1). A rapid surge of ATP subunits was observed over the first 0.5 s, followed by a slightly less rapid replacement with ADP·P_i over the next 2 s, and finally a very slow replacement of ADP·P_i with ADP over the following 58 s. This sequence of events is consistent with Korn et al.'s (1987) model of actin polymerization: first, the initial rate of polymerization far exceeded the constant rate of ATP hydrolysis, so large ATP caps formed; then, as the monomer pool was consumed and polymerization slowed, ATP hydrolysis caught up and the ATP caps were transformed into ADP·P_i caps; finally, random release of inorganic phosphate caused the slow replacement of ADP·P_i subunits with ADP subunits.

The sum of these three curves, yielding the total concentration of polymerized F-actin subunits, predicted a brief

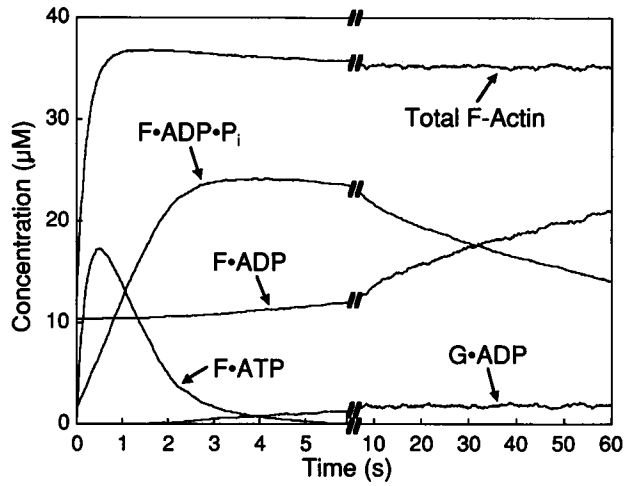

FIGURE 1 Nucleotide composition of polymerized and unpolymerized actin subunits versus time. ATP monomers initially associated rapidly on to filament ends, making ATP subunits the most abundant type for approximately 1 s. This was quickly followed by cleavage of the bound ATP into ADP·P_i. P_i was gradually released over a period of 60 s, leaving ADP subunits as the most abundant species in the filaments.

overshoot of polymerization up to 36.8 μM at 1.7 s, corresponding to a mean filament length of 46 subunits, followed by a slow decay down to a steady value of 35.2 $\pm$ 0.1 μM at 8.5 s, corresponding to a mean filament length of 44 subunits. The prediction of this overshoot by our simulation is consistent with the results reported by Carlier et al. (1985). The decay of the overshoot of F-actin was accompanied by a significant change in the nucleotide composition of the monomer pool. While the concentration of ATP·G-actin fell from an initial value of 25 μM to a steady value of 0.01 $\pm$ 0.01 μM in 5 s, the concentration of ADP·G-actin rose from an initial value of zero to a steady value of 1.8 $\pm$ 0.1 μM by 8.5 s.

The replacement over time of ADP·P_i·F-actin with ADP·F-actin predicted by our simulation is qualitatively consistent with the results reported by Carlier and Pantaloni (1986), but there is a discrepancy between the rates. While the rate of replacement was exponential in both cases as expected for a first order reaction, our data indicate a half-life of 1.4 min as opposed to their value of 2 min. This discrepancy was the first indication in the course of our study that ADP subunits were being incorporated into filaments in an unexpected way. The discrepancy was found to be a result of the formation of ADP caps at the barbed ends of filaments, described further below.

Visualization of the simulation over the time course of polymerization revealed an order in the distribution of nucleotides on filaments. At 0.4 s, long and short ATP caps could be seen at the barbed and pointed ends of filaments, respectively (Fig. 2 *A*). By 8 s these had been replaced by ADP·P_i subunits, and small ADP caps were beginning to appear at the barbed ends (Fig. 2 *B*). Finally, at 60 s, prominent ADP caps could be seen at the barbed ends of many filaments, with a small random distribu-

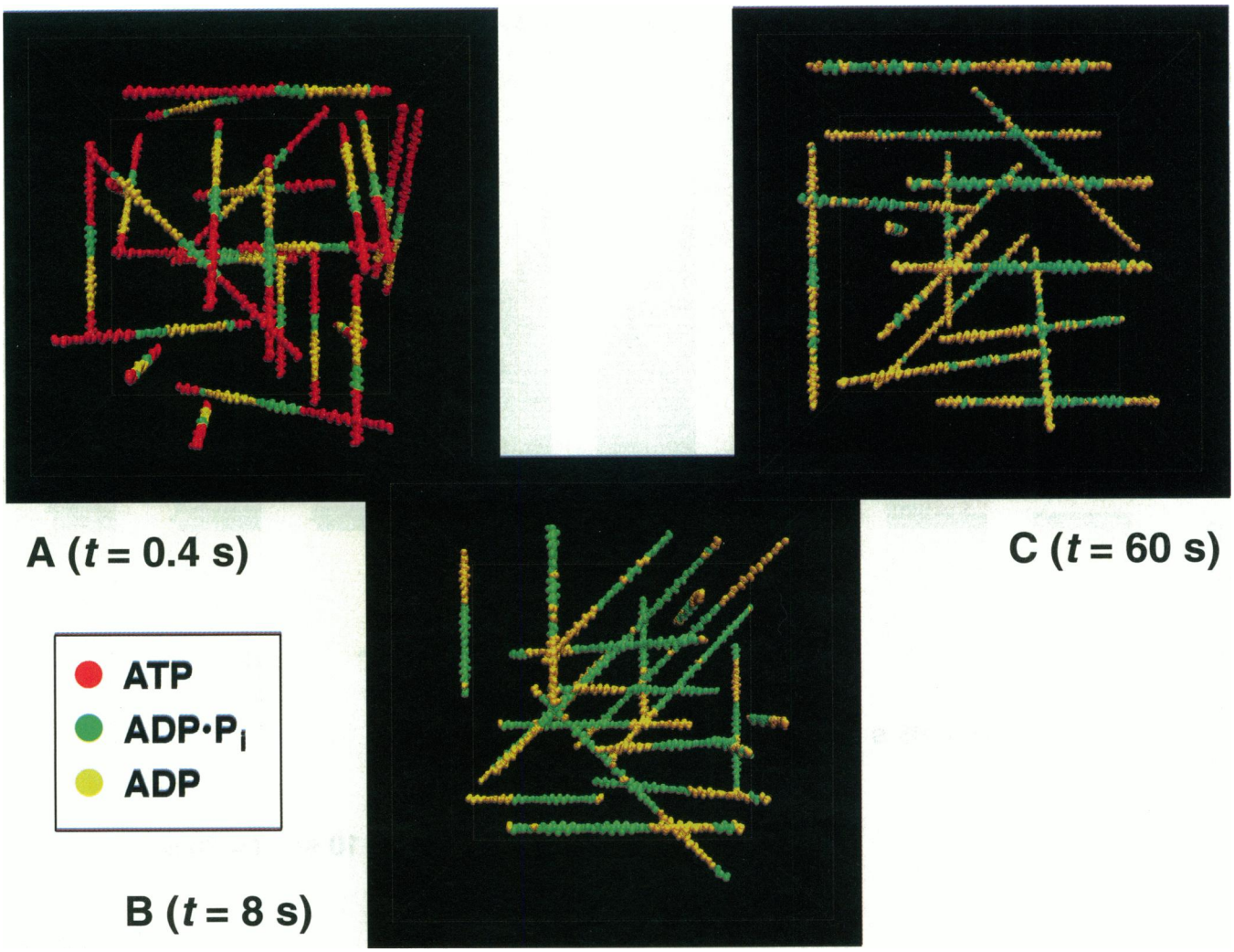

FIGURE 2 Three-dimensional visualization of polymerizing actin filaments at 0.4, 8, and 60 s of model time. The filaments were contained in a cubic lattice whose edges are delineated by thin yellow lines. ATP subunits are red, ADP·P_i subunits are green, and ADP subunits are yellow. (*A*) 0.4 s of model time; (*B*) 8 s; (*C*) 60 s. 80% of the filaments have been chosen at random and removed from the visualization so that the entire length of the remaining filaments can be observed. Large ATP caps appeared at the barbed ends of filaments and smaller caps at the pointed ends after 0.4 s. After 8 s all of the ATP had been cleaved, and ADP·P_i caps occupied both ends of most filaments. Some filaments had small ADP caps at their barbed ends. After 60 s, ADP caps of many sizes could be seen at the barbed ends of filaments, in addition to the expected ADP core near their pointed ends.

tion of ADP sites also appearing inside the ADP·P_i regions (Fig. 2 *C*).

In order to obtain an average representation of the many filaments appearing in the visualizations, the filaments from each saved time step were placed side by side so that the initial filament seeds were aligned. The subunits in each filament were then numbered according to their position n with respect to the initial seed such that $n = 0$ was at the middle of the seed, positive values of n went toward the barbed end of the filament, and negative values went toward the pointed end. For each nucleotide type, all 104 filaments were examined and the number of filaments whose subunit at position n had the specified nucleotide was counted. This procedure revealed the spatial distribution of nucleotides on the filaments (Fig. 3). Large initial distributions of ATP subunits at the barbed and pointed ends of filaments were converted by vectorial hydrolysis into ADP·P_i subunits within 3 s, followed by the appearance of an increasing number of ADP subunits at all positions on the filaments. The distribution of ADP subunits reveals the presence of ADP caps: if the increasing number of ADP subunits was due solely to release of P_i at random locations on the filaments, then the proportion of ADP subunits, taken as a fraction of the total number of subunits at each position, would remain constant. Instead, the proportion of ADP subunits tended toward unity as the ends of the filaments were approached, clearly indicating the presence of ADP caps at both ends of the filaments that were not the result of random P_i release.

The appearance of ADP caps is related to the conversion of the monomer pool to ADP·G-actin noted above. The conversion, explained theoretically by Hill (1981) and demonstrated experimentally by Pantaloni et al. (1984), is due to the presence of high filament concentration and the slow exchange of ADP for ATP on actin monomers (Kinosian et al.,

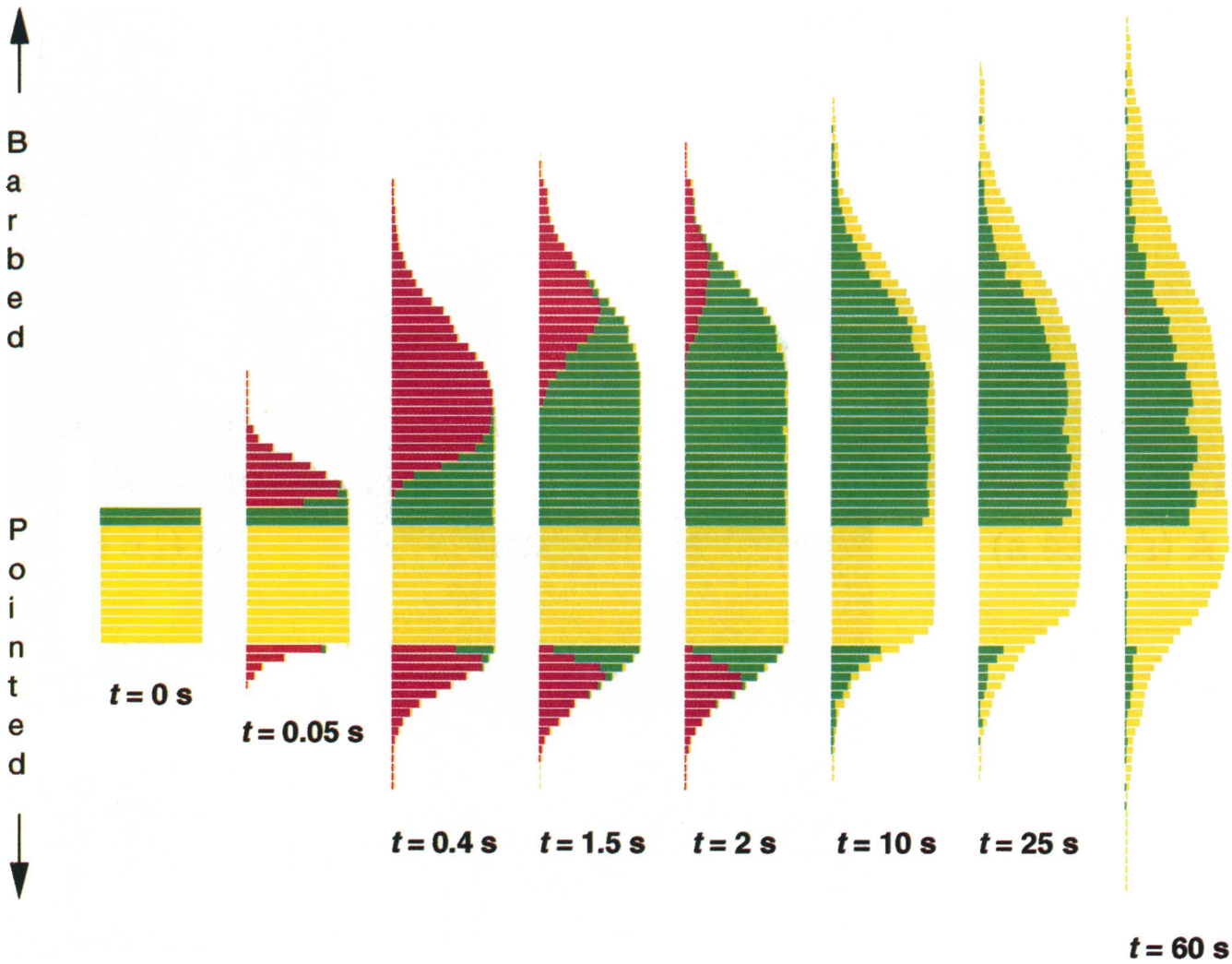

FIGURE 3 Spatial distribution of bound nucleotide on filaments. In order to render the simulation data in this format, the entire contents of the lattice were saved at several time steps throughout the simulation. For each time step, all 104 filaments were positioned side by side so that the initial filament seeds were aligned. This allowed the subunits in each filament to be numbered according to their position n with respect to the initial seed such that n = 0 was at the middle of the seed, positive values of n went toward the barbed end of the filament, and negative values went toward the pointed-end. Each column of bars in the figure is a schematic representation of the filaments from one of the time steps, with each bar corresponding to a different subunit position n. The colors in each bar represent the quantity of each nucleotide type at that position: red is ATP; green is ADP:P_i; and yellow is ADP. The maximum bar length is 104 subunits. All filament seeds began with 13 ADP subunits and 2 ADP·P_i subunits at the barbed end. A large ATP cap quickly grew at the barbed end and was in turn rapidly consumed by vectorial cleavage of ATP to ADP·P_i. A similar but smaller sequence of events occurred simultaneously at the pointed end. Random release of P_i from ADP·P_i subunits then followed, along with growth of a small cap of ADP subunits at the barbed ends of many filaments.

1993). At steady state, when the ends of actin filaments consist of ADP·P_i subunits, association and dissociation of subunits continues but no net change in mean filament length is observed. Under these conditions, the ATP bound to newly associating monomers will be quickly cleaved to ADP·P_i, and when these subunits then dissociate, they are returned to the monomer pool as ADP·G-actin. Once back in the monomer pool, the ADP is eventually released and replaced with ATP, but this exchange proceeds very slowly (from Eq. 3 in Kinosian et al. (1993), k_{ex} = 0.03 s^{-1} for the rate constants and nucleotide concentrations used in the present model). The net result is that the ends of filaments effectively act as conversion sites, binding ATP·G-actin, cleaving the bound ATP, and then releasing the ADP·G-actin and P_i. If the number of filaments is sufficiently high, this conversion overwhelms the monomeric ADP-ATP exchange, and the entire monomer pool is converted to ADP·G-actin, with an accompanying increase in the critical concentration of monomers and partial depolymerization of existing filaments (Pantaloni et al., 1984).

At the time of publication of the work by Pantaloni et al. (1984), it was not yet known that ADP·P_i·F-actin is the primary species found at the barbed ends of filaments at equilibrium, rather than ADP·F-actin (Carlier and Pantaloni, 1986). It was therefore assumed that, once the monomer pool had been converted to ADP·G-actin, both associating and

dissociating subunits would be bound to ADP and therefore the critical concentration would rise to that expected for ADP-actin, as reported in their paper. The supposition of ADP-tipped filaments must be modified, however, to take account of their more recent experiments showing that under conditions of normal filament concentration the equilibrium polymer has ADP·P_i subunits at its barbed ends and not ADP subunits (Carlier and Pantaloni, 1986).

Our simulation results suggest that the appropriate modification consists of the recognition of the existence of ADP caps at the barbed ends of filaments. This conclusion is plausible for the following reasons. If under conditions of high filament concentration the barbed ends of filaments were capped with ADP·P_i subunits rather than ADP subunits, then the associating species would be ADP-actin, but the dissociating species would be ADP·P_i actin which dissociates at the same rate as ATP actin (Korn et al., 1987). The result would be a critical concentration, $C_c = k_{-9}/k_{+11} = 0.2$ μM, which would be lower than the ADP critical concentration, $C_c = k_{-11}/k_{+11} = 2$ μM, since ATP actin dissociates more slowly than ADP actin (Table 1). Pantaloni et al. (1984) reported that the critical concentration under conditions of high filament concentration did in fact approach that of ADP actin, however, so the dissociating species must have been ADP actin, suggesting the presence of ADP caps at the ends of filaments.

If this hypothesis is correct, the concentration of ADP·G-actin under conditions of high filament concentration would be expected to be a function of the concentrations of ADP-tipped filaments $[N_D]$ and ADP·P_i-tipped filaments $[N_P]$, since the barbed ends of the two species have different dissociation rates. At steady state, when filaments have ceased growing, the concentration of ADP·G-actin can be obtained as the ratio of the rate of its production to the rate of its loss,

$$[G_D] = \frac{k_{-9}[N_P] + k_{-11}[N_D] + k_{-12}[N_{tot}]}{(k_{+11} + k_{+12})[N_{tot}] + k_{ex}}, \quad (1)$$

and likewise for the concentration $[G_T]$ of ATP·G-actin,

$$[G_T] = \frac{k_{ex}[G_D]}{(k_{+9} + k_{+10})[N_{tot}]}, \quad (2)$$

where $[N_{tot}]$ is the total concentration of filaments, and $k_{ex} \approx 0.03$ s^{-1} is the rate of exchange of ADP for ATP on actin monomers (other rate constants are defined in Table 1). Equation 1 assumes that the pointed ends of filaments are ADP-tipped (Korn et al., 1987). The data from our simulation support the hypothesis that the concentration of ADP·G-actin depends on the nucleotide composition of the barbed ends of filaments (Fig. 4).

The growth of ADP caps from the ADP-actin monomer pool can be attributed to the microscopic dynamics of the association/dissociation process at the ends of filaments. Hill (1984) and Carlier et al. (1984) have argued that this process consists of F-actin filament length fluctuating back and forth much like the motion of a one-dimensional random walker. They examined the redistribution of ADP·F-actin filament lengths following controlled fragmentation by sonication, and found that the distribution had a Gaussian form that became wider with time as expected for a diffusive system containing many random walkers.

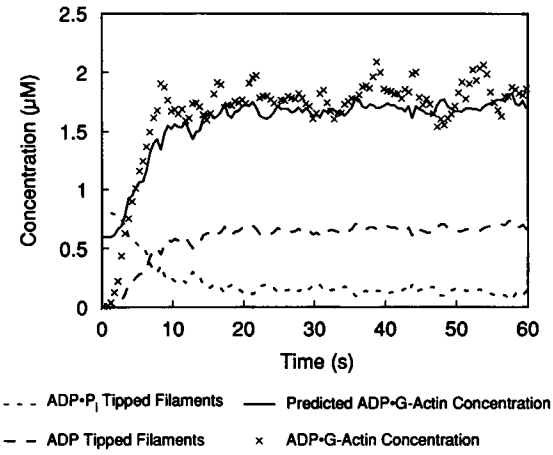

FIGURE 4 Relationship between the concentration of ADP·G-actin and the nucleotide composition of the barbed-end filament tips. The concentration of ADP·G-actin is from the simulation, while the predicted concentration is from Eq. 1 in the text and the concentrations of ADP·P_i-tipped and ADP-tipped filaments from the simulation. Since the dissociation rate of ADP subunits is higher than ADP·P_i subunits, the concentration of ADP·G-actin increases in proportion to the concentration of ADP-tipped filaments.

In our simulation the filament length fluctuations also resulted in a Gaussian distribution (Fig. 5), but were complicated by the presence of ADP·P_i subunits. While lengthening fluctuations of filaments always consisted of association of ADP-actin, shortening fluctuations could consist of either ADP or ADP·P_i dissociations with different rates. Upon completion of polymerization, all filaments were initially capped with ADP·P_i subunits, and all shortening fluctuations therefore consisted of the dissociation of ADP·P_i subunits, adding new ADP·G-actin to the monomer pool. Lengthening fluctuations conversely always consisted of association of ADP subunits to filament ends since the monomer pool contained only ADP·G-actin. The formation of ADP caps at the barbed ends of filaments was therefore directly fed by dissociations from ADP·P_i-tipped filaments.

The prediction of ADP cap growth can be treated as a birth-death process with a reflecting barrier at the origin. Systems behaving as a birth-death process consist of a number (possibly infinite) of discrete states arranged along a line. If such a system is in state n, its only nonzero transition probabilities are for transitions into states $n \pm 1$. A reflecting barrier at the origin implies that a system in state $n = 0$ may only transit to $n = 1$. The time evolution of the probability of a cap of length n at time t is proportional to the probabilities for caps of length $n \pm 1$,

$$\frac{dP_n(t)}{dt} = k_{-11}P_{n+1}(t) + k_{+11}[G_D]P_{n-1}(t) - (k_{-11} + k_{+11}[G_D])P_n(t), \quad (3)$$

while the time evolution of the probability for a capless fila-

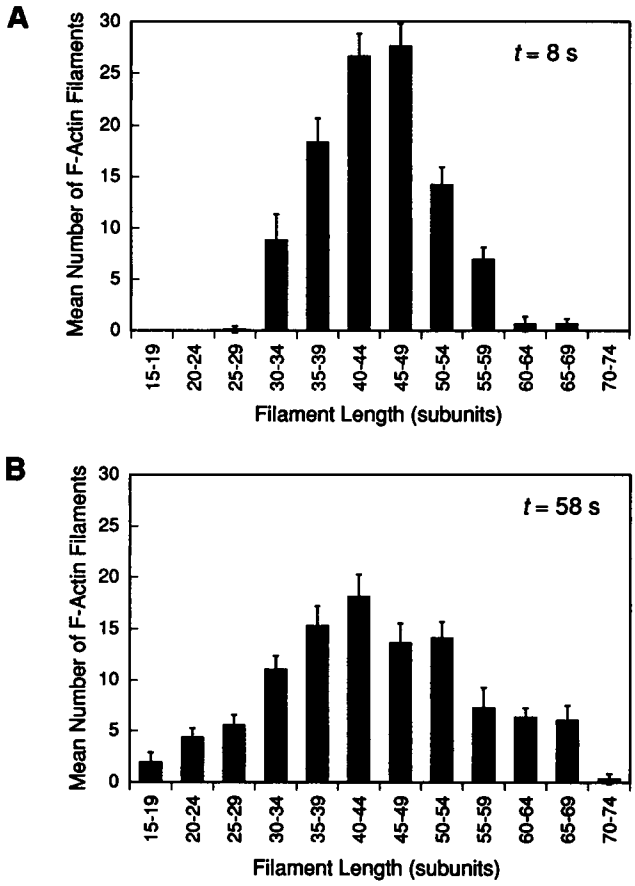

FIGURE 5 Broadening of the Gaussian filament length distribution over time, in agreement with Carlier et al. (1984) random walk model. (*A*) Distribution of filament lengths at 8 s of model time, after polymerization has finished (cf. Fig. 2*B*). (*B*) Distribution of filament lengths after 58 s of model time, at the end of the simulation (cf. Fig. 2*C*). The distribution is much broader than in *A*, as a result of random filament length redistribution over time. The data for each figure were averaged over a period of 4 s of model time centered at 8 s in *A* and 58 s in *B*. Error bars are ±1 S.D. The null hypothesis that the distributions were Gaussian with mean $m = 44$ subunits and variance $s^2 = 48.2$ for *A* and $s^2 = 144.0$ for *B* could not be rejected at a significance of $P < 0.05$ ($\chi^2_{05,6} = 12.6$, $\chi^2_{obs} = 0.5$ for *A*; $\chi^2_{05,10} = 18.3$, $\chi^2_{obs} = 3.4$ for *B*). The mean and variance of both distributions were estimated using the maximum-likelihood method on the original ungrouped data.

ment is proportional only to $P_0(t)$ and $P_1(t)$,

$$\frac{dP_0(t)}{dt} = k_{-11}P_1(t) - k_{+11}[G_D]P_0(t). \quad (4)$$

If we consider the process of ADP cap growth after the concentration of ADP·G-actin has stabilized ($t = 8.5$ s in the present simulation), then Eqs. 3 and 4 imply that

$$P_n(t) = \left(\frac{k_{+11}[G_D]}{k_{-11}}\right)^{(n-1)/2} e^{-(k_{+11}[G_D]+k_{-11})t} \times \left[I_{n-1} + \left(\frac{k_{-11}}{k_{+11}[G_D]}\right)^{1/2} I_{n+2} + \left(1 - \frac{k_{+11}[G_D]}{k_{-11}}\right)\sum_{j=2}^{\infty}\left(\frac{k_{-11}}{k_{+11}[G_D]}\right)^{j/2} I_{n+j+1}\right], \quad (5)$$

where $I_n = I_{-n} = I_n[2(k_{-11}k_{+11}[G_D])^{1/2}t]$ is a modified Bessel function (Goel and Richter-Dyn, 1974), and the fact that the mean ADP cap size in the simulation was 1 subunit at $t = 8.5$ s has been used.

The infinite time limit for the birth-death process yields an expression for the steady-state distribution of ADP caps,

$$P_n(t \to \infty) = \frac{(k_{-11} - k_{+11}[G_D])}{k_{-11}}\left(\frac{k_{+11}[G_D]}{k_{-11}}\right)^n, \quad (6)$$

from which the steady-state mean cap length can be obtained as

$$\langle n \rangle = k_{+11}[G_D]/(k_{-11} - k_{+11}[G_D]). \quad (7)$$

Substitution of $P_0(t \to \infty)$ as $[N_P] = P_0[N_{tot}]$ and $[N_D] = (1 - P_0)[N_{tot}]$ into Eq. 1 gives

$$[G_D] = \frac{k_{-9} + k_{-12}}{k_{+12} + k_{ex}/[N_{tot}] + k_{-9}k_{+11}/k_{-11}} = 1.8\ \mu M, \quad (8)$$

for the expected steady-state concentration of ADP·G-actin as a function of the filament concentration $[N_{tot}]$, in close agreement with the value predicted by our simulation.

Equation 5 describes the time evolution of the ADP cap length in the presence of a pool of pure ADP monomers. Trace amounts of ATP monomers can have a dramatic effect on the ADP cap length distribution, however, since a cap of length n can suddenly be reduced to a cap of length zero by the addition of one ATP subunit. To take account of ATP monomer addition, consider the likelihood that an ADP cap of length n is actually a cap of length $n' < n$ due to the presence of an ATP subunit at $n' + 1$. This likelihood is $(1 - \alpha)\alpha^{n'}$, where $\alpha = k_{+11}[G_D]/(k_{+9}[G_T] + k_{+11}[G_D])$ is the probability that an association onto the barbed end of a filament is an ADP monomer rather than an ATP monomer, and leads to a modified distribution,

$$P'_n(t) = P_n(t)\alpha^n + (1 - \alpha)\alpha^n \sum_{i=n+1}^{\infty} P_i(t), \quad (9)$$

that takes account of the presence of ATP monomers. The modified probability distribution specied by Eq. 9 is in excellent agreement with our simulation results (Fig. 6). The steady-state limit is

$$P'_n(t \to \infty) = \frac{(k_{-11} - \alpha k_{+11}[G_D])}{k_{-11}}\left(\frac{\alpha k_{11}[G_D]}{k_{-11}}\right)^n, \quad (10)$$

and this can again be used to obtain the steady-state mean cap length, modified to take account of the presence of ATP monomers:

$$\langle n \rangle' = \alpha k_{+11}[G_D]/(k_{-11} - \alpha k_{+11}[G_D]). \quad (11)$$

Equation 3 from Kinosian et al. (1993),

$$k_{ex} = \frac{k_{-3}}{1 + k_{+3}[ATP]/k_{+4}[ADP]} + \frac{k_{-4}}{1 + k_{+4}[ATP]/k_{+3}[ADP]}, \quad (12)$$

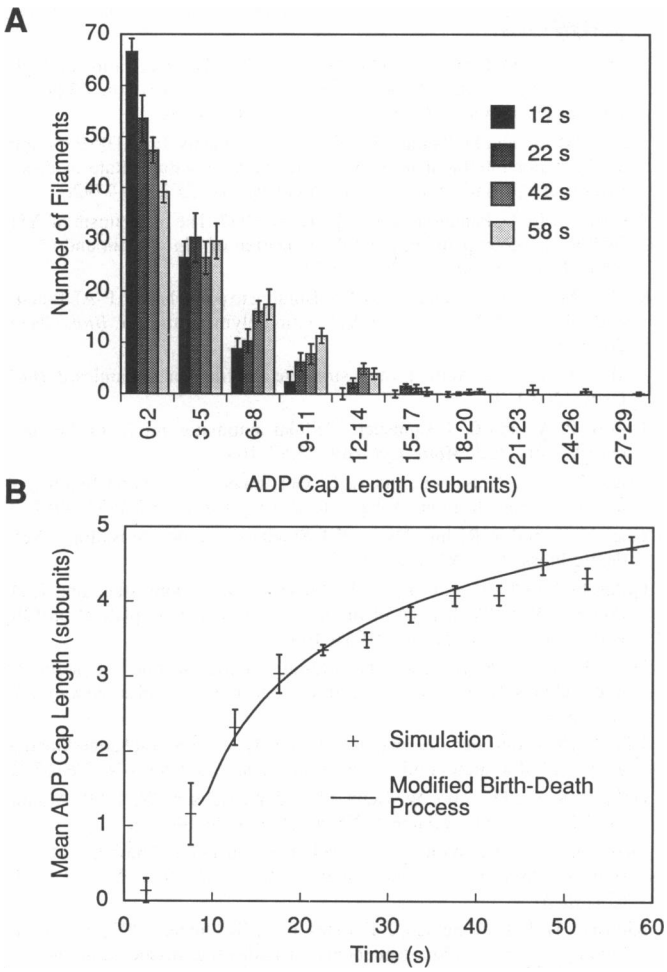

FIGURE 6 (*A*) Length distribution of barbed-end ADP caps at four successive times. Shortening fluctuations at the barbed ends of ADP·P_i-tipped filaments caused new ADP monomers to be added to the monomer pool. Lengthening fluctuations then took up the ADP monomers as ADP caps. The net result was a broadening distribution of longer caps. Each distribution in *A* represents an average over 4 s of model time, centered at the time indicated in the figure. Error bars are ±1 S.D. (*B*) Mean barbed-end ADP cap lengths plotted as a function of time. The rate of incorporation of new ADP subunits into caps decreased as ADP·P_i-tipped filaments were blocked by the association of ADP subunits, causing the rate of increase of the mean cap length to lower with time. Each data point in *B* represents an average over 4 s of model time, centered at the time indicated by the data point's position on the horizontal axis. Since each data point represents the mean of a roughly exponential distribution of cap lengths (see *A*), the standard deviation in each mean cap length measurement is of the order of the mean cap length itself. The null hypothesis that the ADP cap length distributions shown in *A* matched the distribution predicted by Eq. 9 in the text could not be rejected at a significance of $P < 0.05$ (poorest fit was $\chi^2_{.05,5} = 11.1$, $\chi^2_{obs} = 3.3$).

and our Eqs. 2, 8, and 11 can be combined to provide the relationship between the mean length of the exponential steady-state ADP cap-length distribution $\langle n \rangle'$, the ratio of nucleotide concentrations [ATP]/[ADP], and the concentration of F-actin filaments $[N_{tot}]$ (Fig. 7). The mean steady-state ADP cap length approaches zero below $[N_{tot}] = 0.06$ μM, while it diverges rapidly for [ATP]/[ADP] $\rightarrow$ 0.1 and $[N_{tot}] \rightarrow 10$ μM.

This analysis describes the behavior of the barbed ends of filaments. A qualitatively similar sequence of events was in

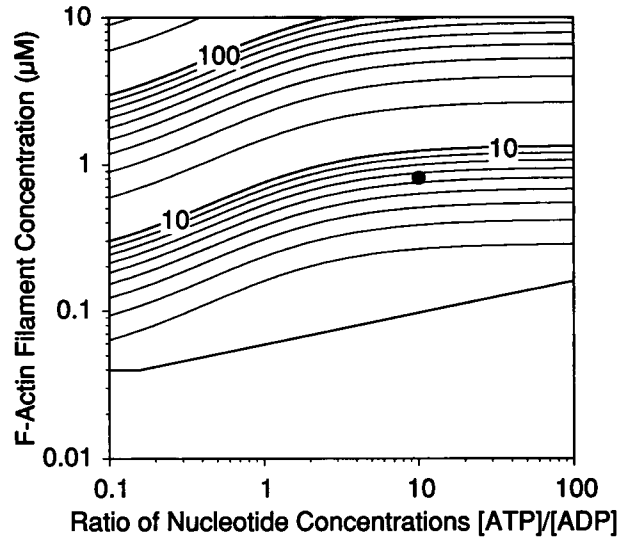

FIGURE 7 Contour plot of mean steady-state barbed-end cap size as a function of nucleotide concentration ratio and F-actin filament concentration. Data for this plot was generated from Eqs. 2, 8, and 11 in the text. The cap size is zero below a filament concentration of approximately 0.06 μM, while the cap size diverges rapidly as the nucleotide ratio [ATP]/[ADP] approaches 0.1 and the filament concentration approaches 10 μM. The large black dot marks the location of the simulation presented in this paper, where the [ATP]/[ADP] ratio is 10, the filament concentration is 0.8 μM, and the resulting steady-state ADP cap size is approximately 6. Note that all values are plotted logarithmically.

fact observed at the pointed ends of filaments as well, but the extent of polymerization, fluctuations, and ADP cap growth was much lower due to the decreased kinetic activity of this end of the filament. Furthermore, fluctuations ate away the small sequence of ADP·P_i subunits at the pointed ends of filaments within only a few seconds of model time, making it difficult to distinguish between those ADP subunits added by fluctuations and those that were present at the beginning of the simulation.

CONCLUSIONS

Filament length redistribution through random length fluctuations will cause the nucleotides on terminal subunits of filaments to reflect the nucleotide composition of the monomer pool. If monomers consist mostly in ATP·G-actin, fluctuations at filament ends will ensure the presence of a cap of ADP·P_i subunits, while an ADP·G-actin pool will result in ADP caps.

This process has the potential to act as a regulator of the F-actin filament population by driving it back and forth between a state of low polymerization and a state of high polymerization. Under conditions associated with cell activation, filament-severing proteins cut filaments into smaller pieces and monomer sequestration proteins release large amounts of G-actin (Stossel, 1989). This results in a substantial increase in the number of filaments followed by massive polymerization, conditions similar to those simulated in the present work. Our findings indicate that, after polymerization has finished, continued fluctuations at filament ends

will cause the progressive widening of the Gaussian distribution of filament lengths, causing some filaments to shrink and disappear (Carlier et al., 1984) while others take up ADP monomers in extended ADP caps.

If monomer-sequestering proteins become reactivated when filaments are in this condition, the monomer concentration will be forced below the critical concentration for ADP-actin. This will cause all ADP capped filaments to depolymerize, dumping all of their ADP subunits back into the monomer pool until the ADP·P_i sequence formed during the initial polymerization phase is reached. The filament population is thus returned to a state of low polymerization, since many filaments will have been lost through filament length redistribution and those left over reduced in size through the loss of their ADP caps. All that is required now to return the cytoskeleton to its preactivation state is the substitution of ATP for ADP on sequestered actin monomers. Kinetic simulations performed by Goldschmidt-Clermont et al. (1991) have suggested that the actin monomer-sequestering protein profilin may actually stimulate this exchange. The process of cycling from low to high polymerization outlined above is plausible given the results we have presented, but more work is required to establish its likelihood in vivo. If it is correct, it likely to be important only in time periods ranging from a few minutes (long enough for the ADP caps to form) to perhaps 30 min. Since the rate of random P_i loss on ADP·P_i·F-actin filaments is k_{-8} = 0.0055 s^{-1} an hour after polymerization has completed all of the F-actin subunits will be bound only to ADP, and loss of filaments through length fluctuations will have reduced the filament concentration to levels incommensurate with ADP caps.

We have presented and discussed the results of a simulation of microfilament polymerization from a solution containing short F-actin seeds and a large concentration of ATP·G-actin. The results are consistent with the model of actin polymerization proposed by Korn et al. (1987), but possess additional characteristics not originally expected from their model: the diffusive formation of ADP caps at the barbed ends of filaments under conditions of high microfilament concentration. We have developed a kinetic model that describes the distribution of ADP cap lengths as a function of nucleotide and filament concentrations, and the model is in excellent agreement with the simulation results. The phenomenon of barbed-end ADP capping appears to be a natural consequence of Korn et al.'s (1987) model and could be important in regulating the characteristics of the F-actin filament population in vivo.

We thank Anthony Zielinski for advice about software development and visualization programming.

This work is supported by funds from the Medical Research Council of Canada (MRC) (to C. J. Lumsden). C. J. Lumsden has been supported by an MRC Career Scientist award. P. A. Dufort holds a Postgraduate Scholarship from the MRC.

REFERENCES

Carlier, M.-F., D. Pantaloni, and E. D. Korn. 1984. Steady state length distribution of F-actin under controlled fragmentation and mechanism of length redistribution following fragmentation. *J. Biol. Chem.* 259:9987–9991.

Carlier, M.-F., D. Pantaloni, and E. D. Korn. 1985. Polymerization of ADP-actin and ATP-actin under sonication and characteristics of the ATP-actin equilibrium polymer. *J. Biol. Chem.* 260:6565–6571.

Carlier, M.-F., and D. Pantaloni. 1986. Direct evidence for ADP·P_i·F-actin as the major intermediate in ATP-actin polymerization. Rate of dissociation of P_i from actin filaments. *Biochemistry.* 25:7789–7792.

Carlier, M.-F., D. Pantaloni, and E. D. Korn. 1987. The mechanism of ATP hydrolysis accompanying the polymerization of Mg^{2+}-actin and Ca^{2+}-actin. *J. Biol. Chem.* 262:3052–3059.

Carlier, M.-F., and D. Pantaloni. 1988. Binding to phosphate to F-ADP-actin and role of F-ADP-P_i actin in ATP-actin polymerization. *J. Biol. Chem.* 263:817–825.

Carlier, M.-F. 1991. Actin: protein structure and filament dynamics. *J. Biol. Chem.* 266:1–4.

Dufort, P. A., and C. J. Lumsden. Cellular automaton model of the actin cytoskeleton. *Cell Motil. Cytoskel.* 25:87–104.

Estes, J. E., L. A. Selden, and L. C. Gershman. 1987. Tight binding of divalent cations to monomeric actin. *J. Biol. Chem.* 262:4952–4957.

Goel, N. S., and N. Richter-Dyn. 1974. Stochastic Models in Biology. Academic Press, New York. pp. 12–31.

Goldschmidt-Clermont, P. J., L. M. Machesky, S. K. Doberstein, and T. D. Pollard. 1991. Mechanism of the interaction of human platelet profilin with actin. *J. Cell Biol.* 113:1081–1089.

Hill, T. 1981. Steady-state head-to-tail polymerization of actin or microtubules II. Two-state and three-state kinetic cycles. *Biophys. J.* 33:353–372.

Hill, T. 1984. Introductory analysis of the GTP-cap phase-change kinetics at the end of a microtubule. *Proc. Natl. Acad. Sci. USA.* 81:6728–6732.

Holmes, K. C., D. Popp, W. Gebhard, and W. Kabsch, W. 1990. Atomic Model of the Actin Filament. *Nature (Lond).* 347:44–49.

Jacobson, K., and J. Wojcieszyn. 1984. The translational mobility of substances within the cytoplasmic matrix. *Proc. Natl. Acad. Sci. USA.* 81: 6747–6751.

Kinosian, H. J., L. A. Selden, J. E. Estes, L. C. Gershman. 1993. Nucleotide binding to actin: cation dependence of nucleotide dissociation and exchange rates. *J. Biol. Chem.* 268:8683–8691.

Korn, E. D. 1982. Actin polymerization and its regulation by proteins from non-muscle cells. *Physiol. Rev.* 62:672–737.

Korn, E. D., M.-F. Carlier, and D. Pantaloni. 1987. Actin polymerization and ATP hydrolysis. *Science (Wash. DC).* 238:638–644.

Kreis, T. E., B. Geiger, and J. Schlessinger. 1982. Mobility of microinjected rhodamine actin within living chicken gizzard cells determined by fluorescence photobleaching recovery. *Cell.* 29:835–845.

Mastro, A. M., M. A. Babich, W. D. Taylor, and A. D. Keith. 1984. Diffusion of a small molecule in the cytoplasm of mammalian cells. *Proc. Natl. Acad. Sci. USA.* 81:3414–3418.

Nowak, E., and R. S. Goody. 1988. Kinetics of adenosine 5′-triphosphate and adenosine 5′-diphosphate interaction with G-actin. *Biochemistry.* 27: 8613–8617.

Oosawa, F., and S. Asakura. 1975. Thermodynamics of the Polymerization of Protein. Academic Press, New York.

Pantaloni, D., M.-F. Carlier, M. Coué, A. A. Lal, S. L. Brenner, and E. D. Korn. The critical concentration of actin in the presence of ATP increases with the number concentration of filaments, and approaches the critical concentration of actin·ADP. *J. Biol. Chem.* 259:6274–6283.

Pollard, T. D., and J. A. Cooper. 1986. Actin and actin-binding processes. A critical evaluation of mechanisms and functions. *Annu. Rev. Biochem.* 55:987–1035.

Pollard, T. D. 1986. Rate constants for the reactions of ATP- and ADP-actin with the ends of actin filaments. *J. Cell Biol.* 103:2747–2754.

Stossel, T. P., C. Chaponnier, R. M. Ezzell, J. H. Hartwig, P. A. Janmey, D. J. Kwiatkowski, S. E. Lind, D. B. Smith, F. S. Southwick, H. L. Yin, and K. S. Zaner. 1985. Nonmuscle actin-binding proteins. *Annu. Rev. Cell Biol.* 1:353–402.

Stossel, T. P. 1989. From signal to pseudopod: how cells control cytoplasmic actin assembly. *J. Biol. Chem.* 264:18261–18264.

Tanford, C. 1961. Physical Chemistry of Macromolecules. John Wiley & Sons, New York. 317–451.